In vivo measurement of brain network connectivity reflects progression and intrinsic disease severity in a model of temporal lobe epilepsy

In vivo measurement of brain network connectivity reflects progression and intrinsic disease severity in a model of temporal lobe epilepsy

Daniele Bertoglio[1,2], Elisabeth Jonckers[3], Idrish Ali[2], Marleen Verhoye[3], Annemie Van der Linden[3], Stefanie Dedeurwaerdere[4,1,*] stefanie.dedeurwaerdere@uantwerpen.be

[1]Molecular Imaging Center Antwerp, University of Antwerp, Belgium

[2]Department of Translational Neurosciences, University of Antwerp, Belgium

[3]Bio-Imaging Lab, University of Antwerp, Belgium

[4]Laboratory of Experimental Hematology, University of Antwerp, Belgium

[*]Corresponding author at: Laboratory of Experimental Hematology, University of Antwerp Universiteitsplein 1, Wilrijk, Antwerp 2610, Belgium.

[1] Current address: UCB Pharma, Rue du Foriest, 1420 Braine l'Alleud, Belgium

Abstract

Different types of brain injury, such as *status epilepticus* (*SE*), trauma, or stroke may initiate the process of epileptogenesis and lead to the development of temporal lobe epilepsy. Epileptogenesis is characterized by an initial latent period during which impaired network communication and synaptic circuit alterations are occurring. Ultimately, these modifications result in the development of spontaneous recurrent seizures (SRS). Current knowledge on the functional connectivity network changes during epileptogenesis and how network alterations relate to seizure is very limited. To investigate these underlying network connectivity modifications, we imaged epileptic and control rats by means of resting-state functional MRI (rsfMRI) during epileptogenesis. A cohort of animals was video-electroencephalography (video-EEG) monitored continuously over 12 weeks to determine disease severity during the course of disease, with the first SRS appearing around 2 weeks post-*SE* for most of the animals. Epileptic animals displayed a significant wide-spread hyposynchrony at 2 weeks post-*SE*, followed by a significant increase in network synchronicity from 2 to 4 weeks post-*SE*. Interestingly, subjects with a delayed epilepsy onset demonstrated significantly lower synchronicity compared to controls and the epileptic group at 4 weeks post-*SE*. Finally, network connectivity at 4 weeks post-*SE* was found to correlate with seizure onset ($r = 0.858$, $p < 0.0001$) and disease severity measured over 12 weeks (e.g. cingulate cortex: $r = 0.863$, $p = 0.002$), suggesting a possible network strengthening upon seizure reoccurrence. Our findings indicate that epileptogenesis is characterized by an initial hyposynchrony of brain networks and the disease-associated progression reflects disease severity.

Keywords: Network connectivity; epileptogenesis; functional MRI; spontaneous recurrent seizure; temporal lobe epilepsy; BOLD response; animal model; rat.

Abbreviations

mTLE mesial temporal lobe epilepsy

SE *status epilepticus*

SRS spontaneous recurrent seizures

rsfMRIresting-state functional MRI

BOLD blood-oxygenation-level-dependent

FC functional connectivity

KASE kainic acid-induced *SE*

video-EEG video-electroencephalography

HC hippocampus

RSC retrosplenial cortex

S1C primary somatosensory cortex

CgC anterior cingulate cortex

Str striatum

S1BFCprimary somatosensory barrel field cortex

DMN-like default-mode-like network, ROI region of interest

PtAC parietal association cortex

PtPC posterior parietal cortex

TeAC temporal association cortex

MC primary motor cortex

Au1C primary auditory cortex

V1C primary visual cortex

EntC entorhinal cortex

InsC insular cortex

PirC piriform cortex

zFC z-transformed functional connectivity

RARE rapid acquisition with relaxation enhancement

FWHM full width at half maximum.

Introduction

Mesial temporal lobe epilepsy (mTLE) with hippocampal sclerosis is the most common form of drug-resistant epilepsy (Tellez-Zenteno and Hernandez-Ronquillo, 2012). mTLE is characterized by abnormal electrical activity in the temporal lobe following an initial injury (such as *status epilepticus* (*SE*), trauma, or stroke), which initiates the process of epileptogenesis and results in the occurrence of spontaneous recurrent seizures (SRS). During epileptogenesis, electrical dysfunction is elicited by the initial injury and it evolves over time, resulting in impaired network communication and synaptic circuit alterations (Lillis et al., 2015).

Electrographic and neuroimaging studies in patients as well as animal models of TLE have led to the concept of epilepsy as a network disorder involving additional connected brain regions beyond the epileptic foci (Bragin et al., 2000; Spencer, 2002). By measuring fluctuations of the blood-oxygenation-level-dependent (BOLD) signal with resting-state functional MRI (rsfMRI), it is possible to monitor non-invasively functional connectivity (FC) between distinct brain regions and elucidate the spatiotemporal evolution of epileptogenesis-related brain FC changes.

RsfMRI has been employed in several studies to investigate alterations in resting-state FC networks in patients with TLE in comparison to healthy controls (Cataldi et al., 2013). On the contrary, only a limited number of preclinical studies have been performed (Bertoglio et al., 2017b). In particular, the majority of preclinical studies are based on traumatic brain injury models, where the development of epileptic seizures is restricted to a limited fraction of the animals. Nonetheless, these preclinical studies described a decrease in FC at the early stage post-injury (Harris et al., 2016b; Mishra et al., 2014; Otte et al., 2012). In addition, a recent study using intrinsic optical imaging in a TLE mouse model reported a reduction in FC during the latent period (Lee et al., 2017). In summary, a growing body of evidence suggests network alterations might be a key component of the pathophysiology of epilepsy. Thus, the main objective of this study was to

investigate whether rsfMRI could detect the underlying maladaptive plasticity occurring during epileptogenesis in an animal model of TLE.

On this basis, we longitudinally investigated FC changes during epileptogenesis by means of rsfMRI. Previous characterization of the SRS profile throughout the progression of the disease in this kainic acid-induced *SE* (KASE) rat model of TLE (Bertoglio et al., 2017a; Bertoglio et al., 2017c) allowed us to select two strategic time points, namely 2 weeks post-*SE*, when most KASE rats are about to experience their first SRS (disease onset), and 4 weeks post-*SE*, when animals have experienced at least one SRS. In addition, we assessed whether network connectivity changes were predictive of epilepsy severity (SRS frequency) measured by continuous long-term video-electroencephalography (video-EEG) during disease progression for a total of 12 weeks.

Materials and methods

Animals

Five weeks old male Wistar Han rats (Charles River Laboratories, France) were individually housed under a 12 h light/dark cycle in a temperature and humidity-controlled environment with food and water available *ad libitum*. The animals were acclimatized for at least 6 days before the start of procedures, which were performed according to the European Committee guidelines (decree 2010/63/CEE) and the Animal Welfare Act (7 USC 2131). All of the experiments were in

compliance with the ARRIVE guidelines and approved by the Ethical Committee for Animal Testing (ECD 2014-39) at the University of Antwerp (Belgium).

Experimental design

A total of 37 rats were included in the study, of which 26 were induced with kainic acid and 11 were included as control animals. Rats were *SE*-induced at 7.5 weeks of age and MRI-scanned during epileptogenesis at 11-14 days post-*SE* (2 weeks post-*SE*), and 27-30 days post-*SE* (4 weeks post-*SE*) (Figure 1) in order to determine changes in functional connectivity by means of rsfMRI. Two different experimental designs were included in the study. During experiment A, both control (n = 11) and KASE rats (n = 14) were included in order to determine network connectivity changes during epileptogenesis and characterize the affected brain networks. During experiment B, only KASE rats were allocated (Figure 1) (n = 12) as this experiment aimed at investigating the relationship between seizures and changes in network connectivity. Animals were implanted with MRI-compatible epidural electrodes 2 weeks before induction of *SE* and were monitored continuously (24/7) with video-EEG during the progression of the disease for 12 weeks in order to assess the SRS frequency for each subject. Animals in experiment B were also investigated for brain inflammation by means of PET imaging with [^{18}F]PBR-111 at the same time points, 2 and 4 weeks post-*SE*. PET and video-EEG results have been published (Bertoglio et al., 2017c).

Electrode implantation

The implantation of the epidural electrodes was performed only for animals allocated to experiment B (n = 12) 2 weeks before the start of the video-EEG recordings (Figure 1) allowing an adequate recovery period as previously described (Bertoglio et al., 2017c). Briefly, animals were anaesthetized (isoflurane: induction 5%, maintenance 2-2.5%; Forene, Belgium) and implanted with

an MRI-compatible epidural tripolar electrode (Bilaney Consultants, Plastics One Inc., Germany) above the parietal cortex. Electrodes were secured to the skull using MRI-compatible materials: nylon anchor screws (Bilaney Consultants, Plastics One Inc., Germany) and dental cement (Simplex Rapid, Kemdent, UK; Durelon, 3M ESPE, USA). At the end of the surgery, xylocaine (2%; AstraZeneca, Belgium) was locally applied to the wound, and buprenorphine (0.01 mg/kg, subcutaneously (s.c.); Ecuphar, the Netherlands) as well as Hartmann's solution (10 ml/kg, s.c.; Viaflo Baxter Healthcare, Belgium) were injected for pain relief and hydration, respectively. The animals were returned to their home cages for recovery while their body temperature was maintained using an infrared lamp and enriched soft food pellets were provided.

Status epilepticus induction

At 7.5 weeks of age, animals were repeatedly administered low-dose injections of KA, as this method has proven its efficacy and has a low mortality rate (Bertoglio et al., 2017a). At *SE* induction, the rats had an average weight of 228 ± 13 g. KASE rats were injected s.c. with an initial dose of 7.5 mg/kg KA (A.G. Scientific, USA) and after 1 h, repetitive injections of 2.5 mg/kg were given every half-hour unless the animal showed seizure behaviour. Injections were repeated until the animals displayed convulsive seizures as previously described (Bertoglio et al., 2017a). All animals reached *SE* after receiving an average dose of 22.7 ± 6.3 mg/kg of KA. During the procedure, the animals were continuously observed and after 4 h of *SE*, diazepam (4 mg/kg; NV Roche SA, Belgium) was administered intraperitoneally (i.p.) to reduce seizures. Control animals received only saline injections (range of 4–6 injections). At the end of the procedure, Hartmann's solution (10 ml/kg, s.c.) was administered to prevent dehydration. Additional care was taken in the days following *SE*, with the animals receiving enriched soft food pellets and Hartmann's solution (10 ml/kg, s.c.). Two rats allocated to experiment A did not survive the procedure (8% mortality rate) and they were excluded from any analysis.

Video-EEG recording and analysis

During experiment A, animals were continuously video-monitored during the whole experiment and video-recordings were analysed by an experienced investigator in order to verify whether KASE rats developed at least one SRS. All KASE rats experienced at least one SRS and the first event was considered the end of the latent period. The median duration of the latent period was 17 days (95% confidence intervals of the mean = 14-21 days). During experiment B, a total of 12 weeks of video-EEG data were collected from freely moving animals as previously described (Bertoglio et al., 2017c). Analysis of video-EEG recordings was performed manually using Neuroscore 3.0 (Data Sciences International, USA) by an experienced investigator as previously described (Amhaoul et al., 2016). In addition to the aberrant EEG-tracing, to be classified as epileptic activity, video-recordings were used to visually determine the severity of the SRS according to the modified scale of Racine (Bertoglio et al., 2017a; Racine, 1972). The latency to the first SRS and the total number of SRS over the recording period (seizure frequency) were quantified.

During the periods the animals were prepared for/recovered from the MRI scan procedure, an experienced investigator constantly monitored the animals for SRS. A total of four SRS were documented during the period following the MR scan, and, importantly, no SRS were recorded during the preparation of the animals. The median duration of the latent period was 17 days (95% confidence intervals of the mean = 15-30 days), while the total number of SRS experienced within the first 4 weeks post-*SE* was 11.1 ± 13.3. The data regarding SRS have been previously published (Bertoglio et al., 2017c).

Magnetic resonance imaging

Procedures

Animals were anaesthetized with isoflurane (Forene, Belgium) in a mixture of N_2/O_2 (70/30%) (induction 5%, maintenance 2-2.5%) and placed in prone position into the scanner with the head fixed in a head holder. Following a bolus injection of 0.05 mg/kg of medetomidine hydrochloride (s.c., 1.2 ml/kg; Domitor, Pfizer, Germany) to sedate the animals, the isoflurane % was gradually decreased to 0%. After 15 min from bolus injection, continuous infusion of medetomidine (0.1 ml/kg/h, s.c.) was started. At the end of the scan, animals received an injection of 0.25 mg/kg of Atipamezole (s.c., 0.5 ml/kg, Antisedan, Pfizer, Germany) to reverse the effects of medetomidine. Previous work has shown that the choice of the anaesthetic can considerably influence the amplitude of the BOLD signal and thus the outcome of functional connectivity studies (Kalthoff et al., 2013; Williams et al., 2010). α-Chloralose sedation has been considered the gold standard in rats, however, its application is limited by toxicity, including possible convulsive effects (Thomas et al., 1988), therefore it cannot be employed for longitudinal studies. On the other hand, isoflurane is a commonly used anaesthetic in rodents, however, it has been shown to mask the naturally occurring network connectivity of the rat brain. A valid alternative is the α2 adrenergic agonist medetomidine. This anaesthetic seems to reduce partially the cortico-striatal connectivity, nonetheless it offers improved BOLD response compared to isoflurane (Kalthoff et al., 2013), allows to perform longitudinal studies, and provides comparable results to the α-Chloralose sedation (Williams et al., 2010). We have previously demonstrated that the dose of medetomidine used in this study showed reliable and reproducible FC in the rat brain (Jonckers et al., 2011). In addition, medetomidine sedation was chosen as it has been proven not to suppress the altered

BOLD response in the epileptic brain, thus appropriate for studying the maturation of epileptogenic networks (Airaksinen et al., 2012). Breathing rate and blood oxygenation were monitored constantly using a pressure sensitive sensor and a pulse oximeter (MR-compatible Small Animal Monitoring and Gating System, SA Instruments, Inc., USA), and remained at normal physiological ranges. A rectal thermistor was inserted to monitor the body temperature, which was maintained at 37 ± 0.5 ºC by means of a feedback-controlled warm air circuitry (MR-compatible Small Animal Heating System, SA Instruments, Inc., USA). MR scans for each animal were performed longitudinally at similar time of the day (mean difference: 31 ± 19 min) in order to avoid possible intra-animal variability due to the daily circadian variation in the brain functional connectivity. The median duration of the time between the last SRS experienced prior MRI scan was 3.1 days (range = 0.9-9.6 days). No relation between this period and the connectivity pattern could be determined.

Data were acquired on a 9.4T Biospec scanner (Bruker, Germany) using a Bruker linear transmit volume coil and a receive-only surface array coil designed for rat head MRI (Jonckers et al., 2011). Three orthogonal multi-slice Turbo Rapid Acquisition with Relaxation Enhancement (RARE) T_2-weighted images were acquired to render slice positioning uniform (repetition time 1500 ms, 12 slices of 1 mm). Field maps were acquired for each scanning session to assess field homogeneity, followed by local shimming, which corrected for the measured inhomogeneity within the brain. Axial rsfMRI scans were acquired 45 min post-bolus injection using a gradient echo EPI (echo planar imaging) sequence (repetition time 2000 ms, echo time 16 ms, 12 slices of 1 mm, slice gap 1.1 mm, 150 repetitions) with a scan duration of 5 min. The field-of-view was 30 x 30 mm^2 and the matrix size 128 x 128, resulting in voxel dimensions of 0.234 x 0.234 x 1 mm^3.

Data preprocessing

Data preprocessing was performed using SPM12 software (Statistical Parametric Mapping, http://www.fil.ion.ucl.ac.uk) in MATLAB 2014a (MathWorks, USA) as previously described

(Jonckers et al., 2011). First, all images within each session were realigned to the first image using a rigid body spatial transformation. Second, datasets were normalized to a study specific EPI template generated by averaging images of all normalized control animals. Next, in plane smoothing was done using a Gaussian kernel with full width at half maximum (FWHM) of twice the pixel size (0.468 x 0.468 mm^2). Finally, a band pass filter (0.01-0.1 Hz) was applied to retain the low frequency fluctuations of the BOLD signal time course. Each individual BOLD time course was visually inspected to exclude the possibility of SRS occurrence during the MRI acquisition.

Data analysis

The first analysis of the data was aimed at identifying relevant functional connectivity maps with a data-driven approach. To this end, we performed an independent component analysis (ICA) (van de Ven et al., 2004) to determine which regions demonstrated to be part of a rsfMRI brain network to include in the second functional connectivity analysis. ICA was performed using the GIFT-Toolbox (Group ICA of fMRI toolbox: http://icatb.sourceforge.net/), by implementing spatial ICA which estimates sources as being statistically spatially independent. This was done in 2 steps, starting with a reduction of the functional data, followed by a concatenation of the data of all animals. Then, a group ICA was performed using the Infomax algorithm. ICA was performed setting the number of components to 15 as previously described (Jonckers et al., 2011). The regional labelling of the different ICA components was performed using the anatomical rat brain atlas (Paxinos and Watson, 2007). A total of 9 neurologically relevant components were identified as shown in Supplementary Figure 1, namely: right hippocampus (HC), retrosplenial cortex (RSC), left cortex, right cortex, primary somatosensory cortex (S1C), anterior cingulate cortex (CgC), striatum (Str), rostral cortex, primary somatosensory barrel field cortex (S1BFC). Based on the anatomical regions comprised in the ICA maps, we selected regions of the default mode-like network (DMN), sensorimotor cortices, and striatum for a region of interest (ROI)-based analysis (Biswal et al., 1995). In addition, during the first exploratory analysis, we included cortical regions characterized by inflammation as we

previously reported that brain inflammation at 2 weeks post-*SE* was predictive of the seizure frequency (Bertoglio et al., 2017c). ROIs were delineated for left and right hemisphere separately using MRIcron software based on the Paxinos and Watson atlas (Paxinos and Watson, 2007) and they included: CgC, parietal association cortex (PtAC), posterior parietal cortex (PtPC), RSC, temporal association cortex (TeAC), dorsal HC, primary motor cortex (MC), primary auditory cortex (Au1C), primary visual cortex (V1C), S1C, entorhinal cortex (EntC), insular cortex (InsC), piriform cortex (PirC), and Str.

The signal time course for each ROI was obtained using REST software. Correlation coefficients between the signal time courses of each pair of ROIs were calculated and *z*-transformed using an *in-house* program developed in MATLAB. The average *z*-transformed correlation values are presented in a functional connectivity (zFC) matrix. The zFC strength of a specific region was calculated as the average of the correlation values between that region and all the other investigated regions. For bilateral regions, the average of the left and right hemispheres was considered for the analysis. The zFC strength in the DMN was determined by calculating the average correlation values between its components (CgC, PtAC, PtPC, RSC, and TeAC) (Hsu et al., 2016), with the exclusion of orbitofrontal and prelimbic cortices due to the higher susceptibility of image artefacts in these regions. Similarly, the zFC strength of the sensorimotor cortices was computed by calculating the average correlation values between its components (MC, Au1C, V1C, and S1C). The zFC strength of the affected brain networks was calculated by selecting only significantly changed networks discovered during the first exploratory analysis. Finally, weighted undirected networks were constructed using BrainNet Viewer (Xia et al., 2013). Nodes were represented by zFC strength of a specific brain region, while edges were determined by the *z*-transformed correlation values between the nodes. Edges with values below 0.5 were not depicted. The diameter of a node indicates its importance within the network, while the thickness of an edge indicates the strength of the functional correlation between the two nodes.

Statistical analysis

Data were assessed for normal distribution using the Shapiro-Wilk normality test. Differences between controls and KASE rats in mean zFC strength were analysed using the repeated measurement 2-way ANOVA test with Bonferroni correction for multiple comparisons testing group and time effect, and their interaction. Due to the limited sample size, the non-parametric Kruskal-Wallis test with Dunn's correction for multiple comparison was used to compare temporal changes in zFC strength among the 3 groups. Spearman's rank correlation test was used to examine the relationship between zFC strength and SRS frequency as well as latency to first SRS in the KASE animals. All of the above-mentioned analyses were performed with GraphPad Prism (v6.0) statistical software. Statistical analysis of the zFC matrices was performed in MATLAB and it included a two sample T-test for comparison between two groups and a paired T-test for comparison within group. False discovery rate correction for multiple comparison was applied to both two sample and paired T-tests. The data are represented as mean ± standard deviation (SD). All tests were two-tailed and significance was set at $p < 0.05$.

Results

Epileptic rats displayed network connectivity hyposynchrony which reverted with disease course

During the first exploratory analysis performed in study cohort A, zFC matrices of KASE rats at 2 weeks post-*SE* revealed an overall statistically significant hyposynchrony in zFC of several brain networks including the DMN-like, sensorimotor cortices, and striatal network (Figure 2A). By comparing the FC between 2 and 4 weeks post-*SE*, we observed a significant increased zFC of KASE rats at 4 weeks post-*SE*, while zFC was not significantly changed in control rats (Supplementary Figure 2).

Mean zFC strength of the DMN-like (Figure 2B) and sensorimotor cortices (Figure 2C) confirmed the significant increase in network connectivity within the KASE rats ($p = 0.0284$ and $p = 0.0031$, respectively). In addition, this analysis confirmed the hyposynchrony in KASE rats at 2 weeks post-*SE* when compared to controls ($p = 0.0016$ and $p = 0.0169$, respectively).

Network connectivity progresses in relation to disease onset

Based on the findings obtained from the exploratory analysis, we investigated network connectivity progression during the disease course by including only regions that displayed significant hyposynchrony at 2 weeks post-*SE*. In addition, since KASE rats did not develop their first SRS at the same time, we divided the epileptic animals in 2 groups depending on the disease onset (first SRS): regular disease onset (<17 days post-*SE*; median = 15, min and max: 13-16 days post-*SE*) and delayed disease onset (≥17 days post-*SE*; median = 21, min and max: 17-27 days post-*SE*).

The mean zFC matrices and representative brain networks of KASE rats with either regular or delayed disease onset were comparable at 2 weeks post-*SE* (Figure 3A-D). Indeed, both KASE groups displayed significant network connectivity hyposynchrony at 2 weeks post-*SE* when compared to controls ($p = 0.0109$ and $p < 0.0001$, respectively) (Figure 3E). Interestingly, the changes in network connectivity at 4 weeks post-*SE* were related to the onset of the disease and they clearly differentiated KASE animals with the regular disease onset rats presenting higher

connectivity as compared to the delayed disease onset animals. Accordingly, animals with regular disease onset showed a significant hypersynchrony at 4 weeks post-*SE* (p = 0.0154), while KASE rats with delayed disease onset remained hyposynchronous (p = 0.0077) as compared to controls (Figure 3E). Finally, the temporal change in KASE rats with regular disease onset was statistically significant (p < 0.0001) (Figure 3E) and confirmed by the significant difference in network connectivity between the two time points (Figure 3F). The profile as well as the temporal change of the mean zFC strength for each region of the identified brain network for each group are shown in Supplementary Figures 3 and 4, respectively.

Network connectivity strength reflects seizure outcome

zFC strength of cingulate cortex during hyposynchrony (2 weeks post-*SE*) was negatively correlating with seizure frequency measured over 12 weeks (r = -0.640, p = 0.0375; median = 0.59 SRS/day and interquartile ranges: 0.47-0.67 SRS/day; Supplementary Table 1) (study cohort B). However, network connectivity strength at 4 weeks post-*SE* positively correlated with seizure frequency in a set of regional networks (e.g. cingulate cortex: r = 0.863, p = 0.002) as depicted in Figure 4. Posterior parietal cortex, hippocampus, and striatum did not show any significant correlation (Supplementary Table 1).

Furthermore, a higher network connectivity strength reflected a shorter seizure onset 4 weeks post-*SE* in all the investigated networks (e.g. cingulate cortex: r = -0.858, p < 0.0001) (Supplementary Table 2 and Figure 5), with the exception of HC. This correlation was not observed for network connectivity strength at 2 weeks post-*SE* (Supplementary Table 2).

Discussion

The present study investigated network connectivity changes during epileptogenesis in the KASE model of temporal lobe epilepsy. Our results showed a wide-spread network connectivity hyposynchrony as well as diverging changes depending on the progression of the disease. Additionally, the network connectivity increase over time reflected seizure onset and disease severity. To our knowledge, this is the first longitudinal study to report resting-state fMRI changes during epileptogenesis in an animal model of temporal lobe epilepsy, to assess network connectivity changes during disease course in combination with long-term continuous video-EEG measurements in the same subjects, and to report a relationship between these measurements.

To date, no longitudinal clinical study investigating changes in network connectivity has been performed, nonetheless several clinical studies have reported FC changes in patients with TLE (Cataldi et al., 2013). In particular, altered resting-state FC has been described in several brain networks including the epileptogenic foci, but also limbic, subcortical and neocortical regions (Caciagli et al., 2014; Rajpoot et al., 2015; Song et al., 2011). Interestingly, resting-state FC of the DMN was found to be altered in patients with TLE (Burianova et al., 2017; Haneef et al., 2014; Liao et al., 2011). Accordingly, in the present study we showed several regions of the DMN being among the most affected during epileptogenesis. Despite the clinical evidences, the DMN received only limited attention at the preclinical level. A recent study using intrinsic optical imaging reported a decrease in intrinsic FC in DMN regions during the latent period in the pilocarpine model of TLE (Lee et al., 2017). This is in line with our findings in the KASE model, however, intrinsic optical signal imaging limits the investigation to cortical regions, thus excluding relevant subcortical regions such as hippocampus (White et al., 2011). Interestingly, decrease in resting-state FC has also been reported in animal models of traumatic brain injury. Mishra and colleagues (2014) described abnormal connectivity between different cortical regions 4 months after lateral fluid-percussion-induced traumatic brain injury. In addition, Harris and colleagues (2016b), investigating the first weeks following controlled cortical impact injury in rats, reported altered FC and suggested

that these network changes might reflect a period of brain functional plasticity (Harris et al., 2016b). Noteworthy, a diffusion tensor imaging study in the same animals showed changes in fractional anisotropy in different brain structures, underlying a potential structural reorganization (Harris et al., 2016a). Accordingly, in a previous study decreases in FC have been reported to concur with changes in fractional anisotropy of white matter in a model of focal epilepsy (Otte et al., 2012). Interestingly, a clinical study describing reduced DMN connectivity in patients with TLE demonstrated that the FC reduction coincided with structural thinning of the white matter fibers in patients with mesial TLE (Liao et al., 2011). In addition, another study demonstrated that functionally linked resting-state networks largely reflect the underlying structural white matter connectivity architecture of the human brain (van den Heuvel et al., 2009). Altogether, our findings and previous reports suggest that following (focal or systemic) epileptogenic insult, changes of functional (and structural) networks are occurring possibly to compensate for the initial insult, and they might lead to a disease-associated maladaptive plasticity. This disease-associated maladaptive plasticity hypothesis is also supported by the correlations between the strength of network connectivity with the duration of the latent period (Figure 5) and the SRS frequency (Figure 4). These findings indicate that animals with shorter disease onset and prone to a higher seizure frequency were characterized by a more pronounced maladaptive plasticity.

In the present study we described epileptogenesis-related changes in connectivity networks in the KASE model of TLE. The interpretation of this FC plasticity is challenging since the underlying biology of its evolution remains speculative. Nonetheless, several biological processes are known to occur following a brain insult such as *SE*. First, a prominent neuronal loss in hippocampal as well as temporal lobe regions, and mossy fiber sprouting take place within the first days post-*SE* (Bertoglio et al., 2017a; Gorter et al., 2001; Pitkanen et al., 2002). Also, we previously reported high levels of gliosis in this animal model at the same time points investigated in the present study (Amhaoul et al., 2015; Bertoglio et al., 2017c). In addition, blood-brain barrier leakage occurs during

epileptogenesis (van Vliet et al., 2007) and it has been reported to lead to neurovascular remodelling (Bankstahl et al., 2018) as well as inflammation-related excitability, and ultimately progression of epilepsy (van Vliet et al., 2007; Vezzani et al., 2011). The majority of these processes peaks around 1 to 2 weeks post-*SE* and they show a trend towards resolving over time before chronic disease (Pitkanen et al., 2018). It is likely that the combination of all these processes is responsible for the functional (and structural) changes leading to the reorganization of the connectivity networks. Despite that, future studies are needed to underpin which might be the primary contributor responsible for the network connectivity alterations occurring during epileptogenesis.

In conclusion, we observed brain network connectivity hyposynchrony during epileptogenesis, which might represent a potential biomarker to test antiepileptogenic therapies. In addition, we demonstrated diverging changes in network connectivity being related to the disease onset and we showed that network connectivity reflects seizure onset and disease severity, offering a predictive readout on the progression of the disease. Although future studies are needed to identify the underlying mechanisms involved in resting-state FC changes, our findings offer insights in the pathological changes of the local and remote brain network occurring during epileptogenesis with the potential for translational application.

Acknowledgements

The authors would like to thank Krystyna Szewczyk and Johan Van Audekerke for the valuable technical laboratory support and assistance.

Funding

D.B. has a PhD fellowship from the Research Foundation Flanders (FWO, 11W2516N/11W2518N). S.D. is supported by Research Foundation Flanders (FWO) funding 1.5.110.14N, 1.5.144.12N and ERA-NET NEURON G.A009.13N, and finally by Queen Elisabeth Medical Foundation (Q.E.M.F.) for Neurosciences. E.J. has a post-doctoral fellowship from the Research Foundation Flanders (FWO, 12R1917N).

Declaration of interest

None.

Appendix A. Supplementary data

Supplementary data to this article can be found online.

References

Airaksinen, A. M., et al., 2012. Simultaneous BOLD fMRI and local field potential measurements during kainic acid-induced seizures. Epilepsia. 53**,** 1245-53.

Amhaoul, H., et al., 2016. P2X7 receptor antagonism reduces severity of spontaneous seizures in a chronic model of temporal lobe epilepsy. Neuropharmacology.

Amhaoul, H., et al., 2015. Brain inflammation in a chronic epilepsy model: Evolving pattern of the translocator protein during epileptogenesis. Neurobiol Dis. 82**,** 526-39.

Bankstahl, M., et al., 2018. Blood-Brain Barrier Leakage during Early Epileptogenesis Is Associated with Rapid Remodeling of the Neurovascular Unit. eNeuro. 5.

Bertoglio, D., et al., 2017a. Kainic Acid-Induced Post-Status Epilepticus Models of Temporal Lobe Epilepsy with Diverging Seizure Phenotype and Neuropathology. Front neurol. 8.

Bertoglio, D., et al., 2017b. Neuroimaging in animal models of epilepsy. Neuroscience. 358**,** 277-299.

Bertoglio, D., et al., 2017c. Non-invasive PET imaging of brain inflammation at disease onset predicts spontaneous recurrent seizures and reflects comorbidities. Brain Behav Immun. 61**,** 69-79.

Biswal, B., et al., 1995. Functional connectivity in the motor cortex of resting human brain using echo-planar MRI. Magn Reson Med. 34**,** 537-41.

Bragin, A., et al., 2000. Chronic epileptogenesis requires development of a network of pathologically interconnected neuron clusters: a hypothesis. Epilepsia. 41 Suppl 6**,** S144-52.

Burianova, H., et al., 2017. Altered functional connectivity in mesial temporal lobe epilepsy. Epilepsy Res. 137**,** 45-52.

Caciagli, L., et al., 2014. Functional network alterations and their structural substrate in drug-resistant epilepsy. Front Neurosci. 8**,** 411.

Cataldi, M., et al., 2013. Resting state networks in temporal lobe epilepsy. Epilepsia. 54**,** 2048-59.

Gorter, J. A., et al., 2001. Progression of spontaneous seizures after status epilepticus is associated with mossy fibre sprouting and extensive bilateral loss of hilar parvalbumin and somatostatin-immunoreactive neurons. Eur J Neurosci. 13**,** 657-69.

Haneef, Z., et al., 2014. Network analysis of the default mode network using functional connectivity MRI in Temporal Lobe Epilepsy. J Vis Exp. e51442.

Harris, N. G., et al., 2016a. Bi-directional changes in fractional anisotropy after experiment TBI: Disorganization and reorganization? Neuroimage. 133**,** 129-143.

Harris, N. G., et al., 2016b. Disconnection and hyper-connectivity underlie reorganization after TBI: A rodent functional connectomic analysis. Exp Neurol. 277**,** 124-138.

Hsu, L. M., et al., 2016. Constituents and functional implications of the rat default mode network. Proc Natl Acad Sci U S A. 113**,** E4541-7.

Jonckers, E., et al., 2011. Functional connectivity fMRI of the rodent brain: comparison of functional connectivity networks in rat and mouse. PLoS One. 6**,** e18876.

Kalthoff, D., et al., 2013. Reliability and spatial specificity of rat brain sensorimotor functional connectivity networks are superior under sedation compared with general anesthesia. NMR Biomed. 26**,** 638-50.

Lee, H., et al., 2017. Altered intrinsic functional connectivity in the latent period of epileptogenesis in a temporal lobe epilepsy model. Exp Neurol. 296**,** 89-98.

Liao, W., et al., 2011. Default mode network abnormalities in mesial temporal lobe epilepsy: a study combining fMRI and DTI. Hum Brain Mapp. 32**,** 883-95.

Lillis, K. P., et al., 2015. Evolution of Network Synchronization during Early Epileptogenesis Parallels Synaptic Circuit Alterations. J Neurosci. 35**,** 9920-34.

Mishra, A. M., et al., 2014. Decreased resting functional connectivity after traumatic brain injury in the rat. PLoS One. 9**,** e95280.

Otte, W. M., et al., 2012. Characterization of functional and structural integrity in experimental focal epilepsy: reduced network efficiency coincides with white matter changes. PLoS One. 7**,** e39078.

Paxinos, G., Watson, C., 2007. The rat brain in stereotaxic coordinates. Elsevier Inc. . 456.

Pitkanen, A., et al., 2018. Epilepsy biomarkers - Toward etiology and pathology specificity. Neurobiol Dis.

Pitkanen, A., et al., 2002. Progression of neuronal damage after status epilepticus and during spontaneous seizures in a rat model of temporal lobe epilepsy. Prog Brain Res. 135**,** 67-83.

Racine, R. J., 1972. Modification of seizure activity by electrical stimulation. II. Motor seizure. Electroencephalogr Clin Neurophysiol. 32**,** 281-94.

Rajpoot, K., et al., 2015. Functional Connectivity Alterations in Epilepsy from Resting-State Functional MRI. PLoS One. 10**,** e0134944.

Song, M., et al., 2011. Impaired resting-state functional integrations within default mode network of generalized tonic-clonic seizures epilepsy. PLoS One. 6**,** e17294.

Spencer, S. S., 2002. Neural networks in human epilepsy: evidence of and implications for treatment. Epilepsia. 43**,** 219-27.

Tellez-Zenteno, J. F., Hernandez-Ronquillo, L., 2012. A review of the epidemiology of temporal lobe epilepsy. Epilepsy Res Treat. 2012**,** 630853.

Thomas, H. M., et al., 1988. The Toxic Effects of Alpha-Chloralose. Human Toxicology. 7**,** 285-287.

van de Ven, V. G., et al., 2004. Functional connectivity as revealed by spatial independent component analysis of fMRI measurements during rest. Hum Brain Mapp. 22**,** 165-78.

van den Heuvel, M. P., et al., 2009. Functionally linked resting-state networks reflect the underlying structural connectivity architecture of the human brain. Hum Brain Mapp. 30**,** 3127-41.

van Vliet, E. A., et al., 2007. Blood-brain barrier leakage may lead to progression of temporal lobe epilepsy. Brain. 130**,** 521-34.

Vezzani, A., et al., 2011. The role of inflammation in epilepsy. Nat Rev Neurol. 7**,** 31-40.

White, B. R., et al., 2011. Imaging of functional connectivity in the mouse brain. PLoS One. 6**,** e16322.

Williams, K. A., et al., 2010. Comparison of alpha-chloralose, medetomidine and isoflurane anesthesia for functional connectivity mapping in the rat. Magn Reson Imaging. 28**,** 995-1003.

Xia, M., et al., 2013. BrainNet Viewer: a network visualization tool for human brain connectomics. PLoS One. 8**,** e68910.

Figure legends

Figure 1 Study design. Schematic diagram of the experiments performed. In experiment A, controls (n = 11) and KASE animals (n = 14) were included to determine functional connectivity changes during epileptogenesis. Resting-state fMRI scans were acquired at 2 and 4 weeks post-*SE*. Animals were video monitored to confirm the development of spontaneous recurrent seizures. Experiment B aimed at investigating the relationship between changes in functional connectivity and SRS outcome, thus only KASE rats (n = 12) were included. MR-compatible electrodes were implanted 2 weeks before *SE* and video-EEG monitoring was performed continuously during all stages of the disease (acute, latent and chronic epilepsy) for 12 weeks in order to assess the SRS frequency for each subject. *SE* induction and resting-state fMRI acquisition were performed at the same age and time points as for experiment A. *SE* = status epilepticus; KASE = kainic acid-induced *SE*; fMRI = functional MRI.

Figure 2 KASE rats initially displayed wide-spread reduction in network connectivity which reverted with disease course. Mean z-transformed FC strength matrices of controls (lower half) and KASE rats (upper half) showed a statistically significant hyposynchrony in network connectivity of KASE rats at 2 weeks post-*SE* (**A**). The colour scale represents the strength of the functional correlation between pairs of brain regions. Statistically significant (false discovery rate corrected) changes in pairs of brain regions between groups are indicated with * in the upper half. The specific brain regions are (from top to bottom): anterior cingulate cortex (CgC), parietal association cortex (PtAC), posterior parietal cortex (PtPC), retrosplenial cortex (RSC), temporal association cortex (TeAC), dorsal hippocampus (HC), primary motor cortex (MC), primary auditory cortex (Au1C), primary visual cortex (V1C), primary somatosensory cortex (S1C), entorhinal cortex (EntC), insular cortex (InsC), piriform cortex (PirC), and striatum (Str). Mean zFC strength within the default-mode-like network (B) and within sensorimotor cortices (C) showed a significant increase in network connectivity strength with the progression of the disease. *$p < 0.05$, **$p < 0.01$. Only significance within group is shown. Controls (n = 11), KASE rats (n = 12). Animals from experiment A are included. *SE* = status epilepticus, L = left, R = right, DMN = default-mode-like network.

Figure 3 Network connectivity progression was related to disease onset. (A) KASE rats with regular disease onset displayed a significant temporal increase in the mean z-transformed FC (zFC) of the identified affected brain networks **(A)**, also visible in the representative related networks **(B)**. On the contrary, KASE rats with delayed disease onset showed only limited significant temporal changes in zFC matrices **(C)** or related networks **(D)**. While all KASE rats were characterized by statistically significant hyposynchrony at 2 weeks post-*SE*, only KASE rats with regular disease onset displayed a temporal change **(E)**. The different in zFC strength between the two time points was significantly increased in the KASE rats with regular disease onset compared to the other groups **(F)**. *$p < 0.05$, **$p < 0.01$, ****$p < 0.0001$. Controls ($n = 11$), KASE regular onset ($n = 7$), KASE delayed onset ($n = 5$). The colour scale of zFC maps represents the strength of the functional correlation between pairs of brain regions. Statistically significant (false discovery rate corrected) changes in pairs of brain regions between groups are indicated with * in the upper half. In B and D, the diameter of a node indicates its importance within the network, while the thickness of an edge indicates the strength of the functional correlation between the 2 nodes. Animals from experiment A are included. CgC = anterior cingulate cortex, PtAC = parietal association cortex, PtPC = posterior parietal cortex, HC = dorsal hippocampus, MC = primary motor cortex, S1C = primary somatosensory cortex, Str = striatum, L = left, R = right.

Figure 4 Stronger network connectivity strength at 4 weeks post-*SE* reflected higher seizure frequency. Mean FC strength of the affected brain networks at 4 weeks post-*SE* significantly correlated with SRS frequency measured over 12 weeks post-*SE*. Spearman's rank correlation. Animals from experiment B are included. Note the logarithmic scale on the x-axis. zFC = z-score functional connectivity.

Figure 5 Network connectivity strength reflected seizure onset. Mean FC strength of affected brain networks at 4 weeks post-*SE* significantly correlated with the duration of the latent period for both experiments A and B. Spearman's rank correlation. Note the logarithmic scale on the x-axis. Animals from experiments A and B are included. zFC = z-score functional connectivity.

Supplementary Figure 1 Relevant functional connectivity maps resulting from 15 components ICA. A total of nine neurologically relevant mean components were identified. Each component was determined including both KASE and control animals and it is represented by colour-coded z-maps overlaid onto the GE-EPI template presenting the anatomical area. A higher z-score represents a higher correlation between the time course of that voxel and the mean time course of the component. The components are: right hippocampus (**A**), retrosplenial cortex (**B**), left cortex (**C**), right cortex (**D**), primary somatosensory cortex (**E**), anterior cingulate cortex (**F**), striatum (**G**), rostral cortex (**H**), primary somatosensory barrel field cortex (**I**).

Supplementary Figure 2 Temporal evolution of network connectivity in controls and KASE rats. Mean z-transformed FC at 2 (upper half) and 4 (lower half) weeks post-*SE* for controls (**A**) and KASE rats (**B**). The colour scale represents the strength of the functional correlation between pairs of brain regions. Statistically significant (false discovery rate corrected) changes in network connectivity between 2 and 4 weeks post-*SE* are indicated with an * in the upper half. The specific brain regions are (from top to bottom): anterior cingulate cortex (CgC), parietal association cortex (PtAC), posterior parietal cortex (PtPC), retrosplenial cortex (RSC), temporal association cortex (TeAC), dorsal hippocampus (HC), primary motor cortex (MC), primary auditory cortex (Au1C), primary visual cortex (V1C), primary somatosensory cortex (S1C), entorhinal cortex (EntC), insular cortex (InsC), piriform cortex (PirC), and striatum (Str). Controls (n = 11), KASE rats (n = 12). L = left, R = right.

Supplementary Figure 3 Network connectivity strength of the affected brain networks. Mean zFC strength was significantly reduced in both regular and delayed onset KASE rats at 2 weeks post-*SE* when compared to controls. At 4 weeks post-*SE,* KASE rats with regular disease onset showed a significantly increased zFC strength in all regions of the identified affected brain networks. KASE rats with delayed disease onset still displayed a significant decreased zFC strength compared to controls. *p < 0.05, **p < 0.01, ***p < 0.001, ****p < 0.0001. Controls (n = 11), KASE regular onset (n = 7), KASE delayed onset (n = 5). zFC = z-score functional connectivity.

Supplementary Figure 4 Temporal change in network connectivity strength of the affected brain networks. KASE rats with regular disease onset were characterized by a significant overall increase in mean zFC strength between 4 and 2 weeks post-*SE* when compared to the other groups, with the exception of hippocampus. *$p < 0.05$, **$p < 0.01$, ***$p < 0.001$. Controls ($n = 11$), KASE regular onset ($n = 7$), KASE delayed onset ($n = 5$). zFC = z-score functional connectivity.

Highlights

- Epileptic rats display network connectivity hyposynchrony during epileptogenesis.
- Network connectivity changes over time are related to disease onset.
- Network connectivity strength correlates with seizure onset and disease severity.
- RsfMRI during epileptogenesis offers a predictive readout on disease progression.

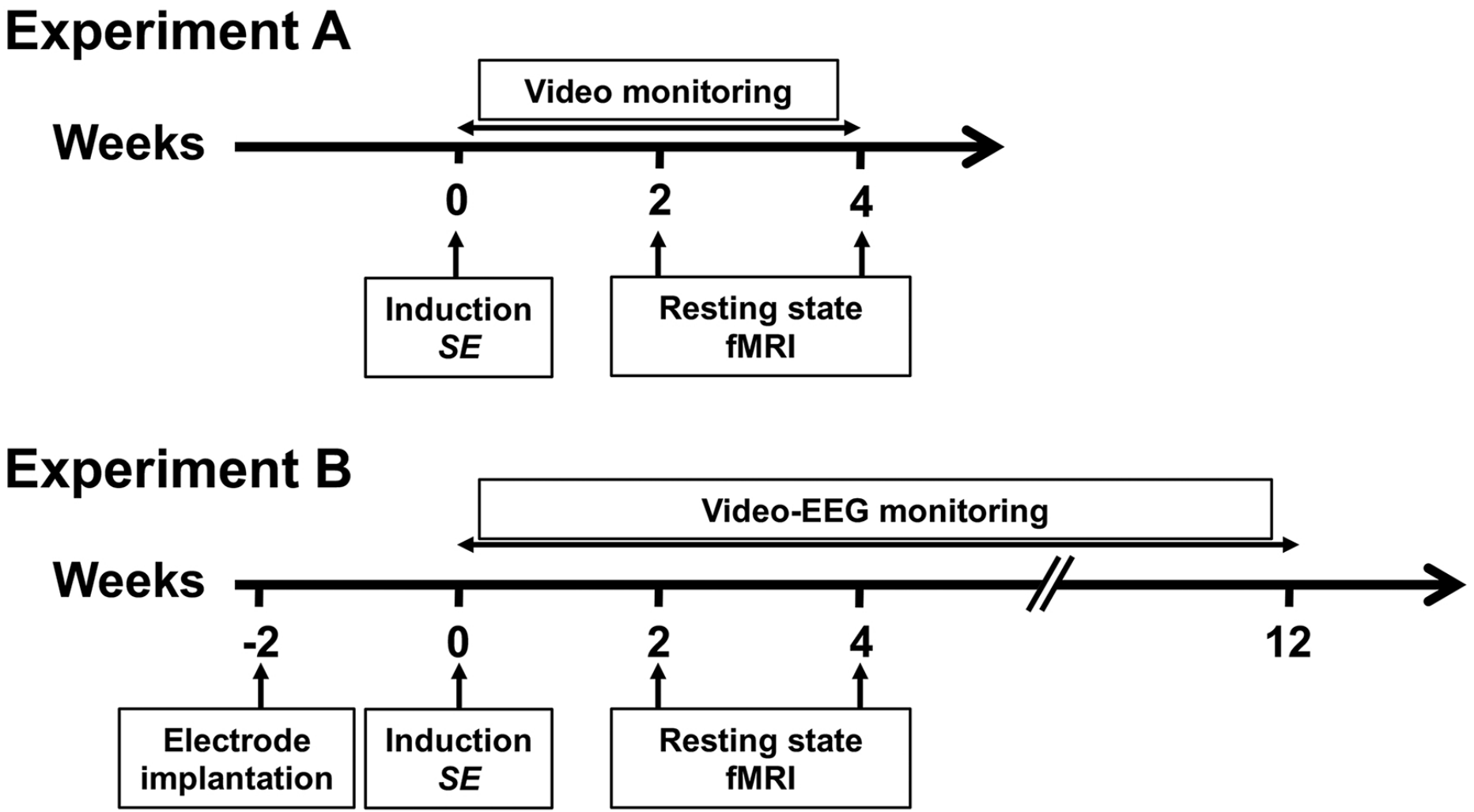
Experiment A
Video monitoring
Weeks
0
2
4
Induction
SE
Resting state
fMRI
Experiment B
Video-EEG monitoring
Weeks
-2
0
2
4
12
Electrode
implantation
Induction
SE
Resting state
fMRI

Figure 1

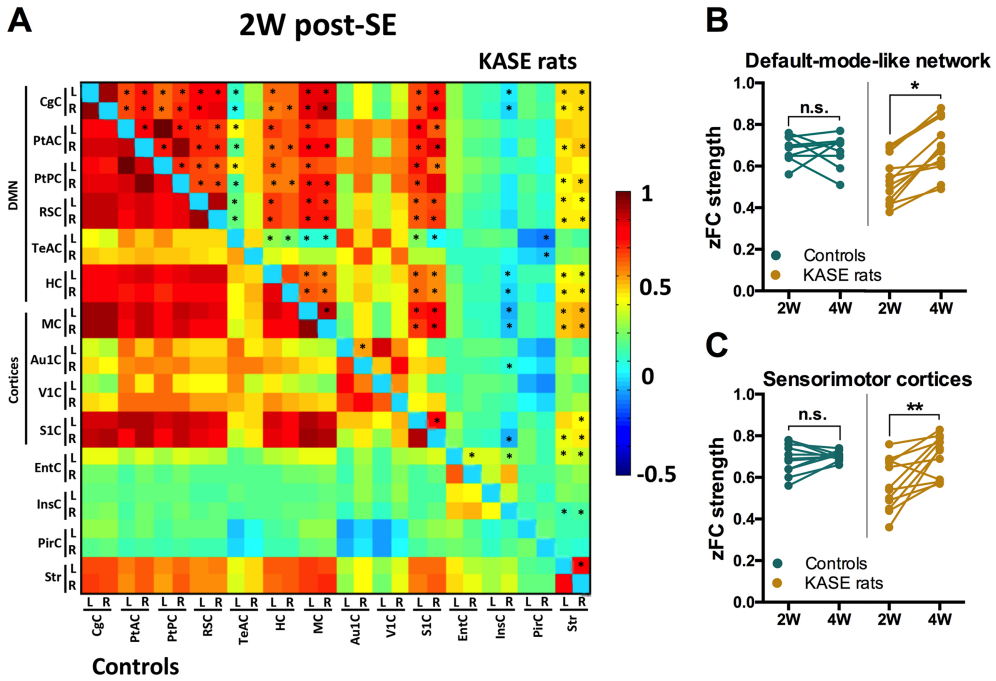
A
2W post-SE
KASE rats
DMN
Cortices
CgC
PtAC
PtPC
RSC
TeAC
HC
MC
Au1C
V1C
S1C
EntC
InsC
PirC
Str
L
R
1
0.5
0
-0.5
Controls
B
Default-mode-like network
zFC strength
n.s.
*
Controls
KASE rats
2W
4W
C
Sensorimotor cortices
**

Figure 2

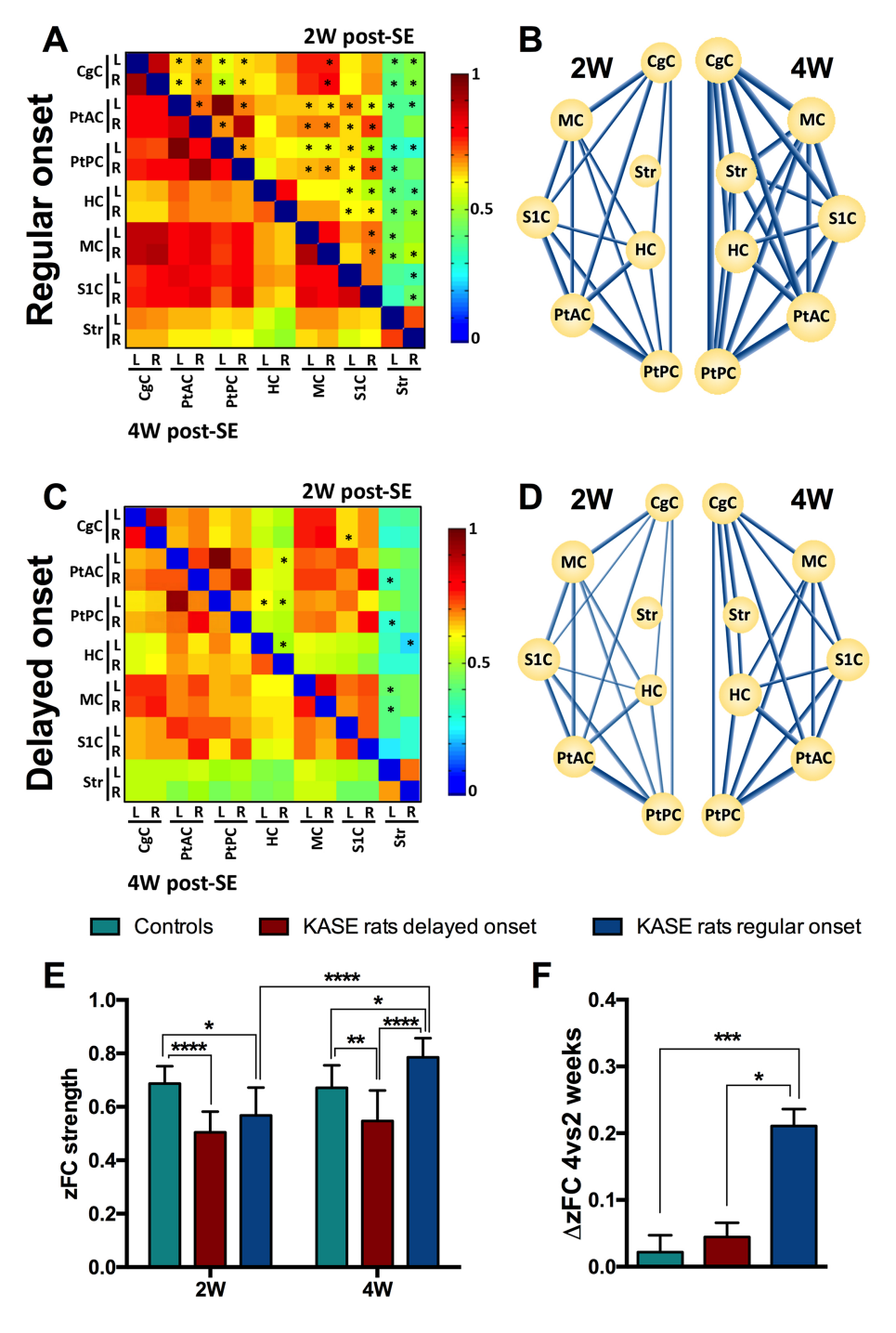
A
2W post-SE
Regular onset
CgC
PtAC
PtPC
HC
MC
S1C
Str
L R
1
0.5
0
4W post-SE
B
2W
4W
CgC
MC
Str
S1C
HC
PtAC
PtPC
C
2W post-SE
Delayed onset
4W post-SE
D
2W
4W
Controls
KASE rats delayed onset
KASE rats regular onset
E
zFC strength
1.0
0.8
0.6
0.4
0.2
0.0
2W
4W
****
*
**
F
ΔzFC 4vs2 weeks
0.4
0.3
0.2
0.1
0.0
***
*

Figure 3

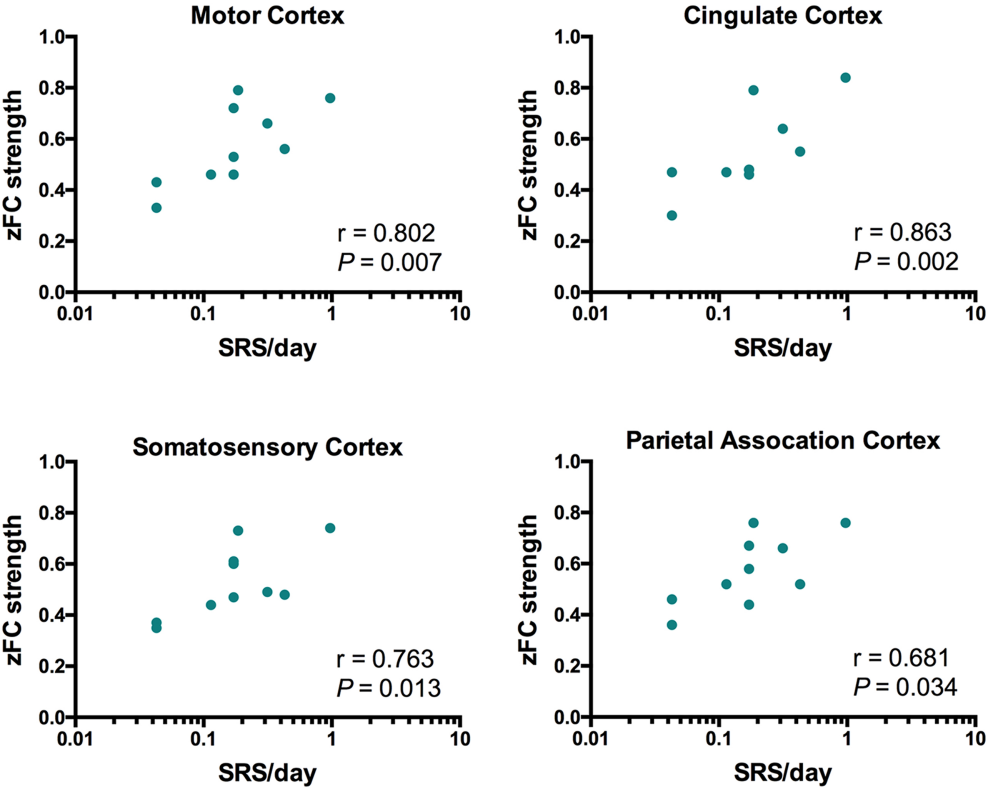
Motor Cortex
zFC strength
SRS/day
r = 0.802
P = 0.007
Cingulate Cortex
zFC strength
SRS/day
r = 0.863
P = 0.002
Somatosensory Cortex
zFC strength
SRS/day
r = 0.763
P = 0.013
Parietal Assocation Cortex
zFC strength
SRS/day
r = 0.681
P = 0.034

Figure 4

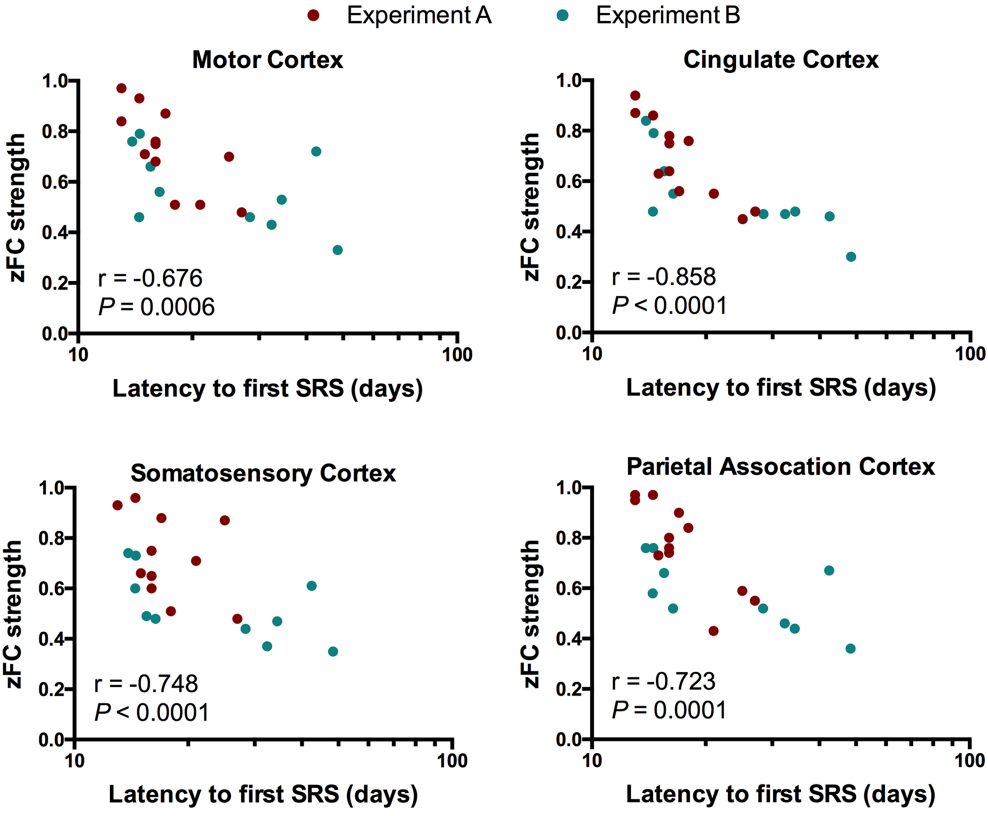
Experiment A
Experiment B
Motor Cortex
zFC strength
r = -0.676
P = 0.0006
Latency to first SRS (days)
Cingulate Cortex
zFC strength
r = -0.858
P < 0.0001
Latency to first SRS (days)
Somatosensory Cortex
zFC strength
r = -0.748
P < 0.0001
Latency to first SRS (days)
Parietal Assocation Cortex
zFC strength
r = -0.723
P = 0.0001
Latency to first SRS (days)

Figure 5

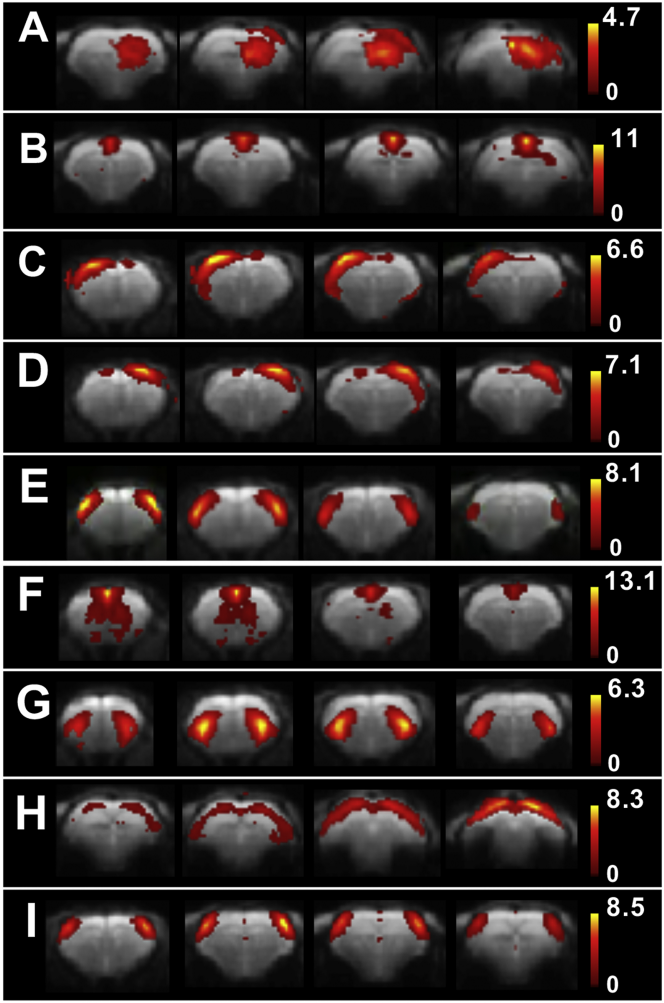

Figure 6

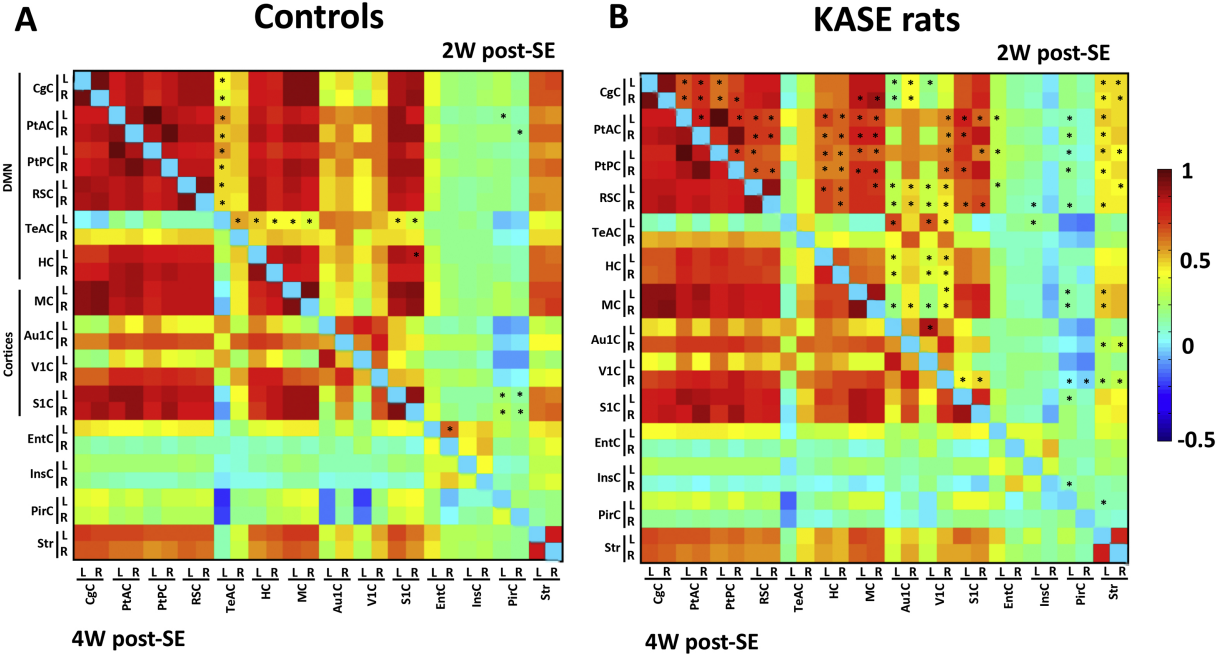
A
Controls
2W post-SE
B
KASE rats
2W post-SE
DMN
Cortices
CgC
PtAC
PtPC
RSC
TeAC
HC
MC
Au1C
V1C
S1C
EntC
InsC
PirC
Str
L
R
1
0.5
0
-0.5
4W post-SE
4W post-SE

Figure 7

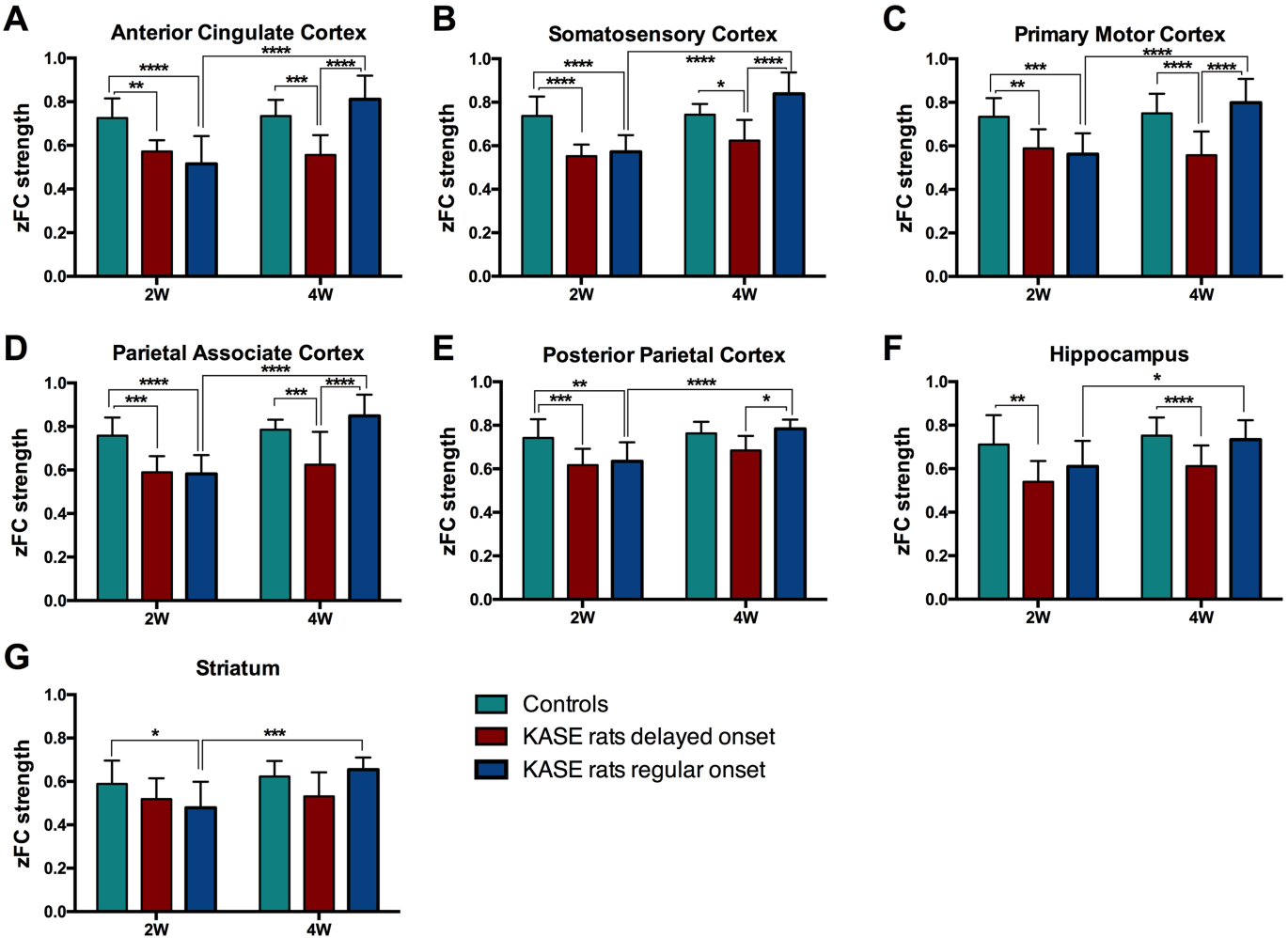
A
Anterior Cingulate Cortex
B
Somatosensory Cortex
C
Primary Motor Cortex
D
Parietal Associate Cortex
E
Posterior Parietal Cortex
F
Hippocampus
G
Striatum
zFC strength
1.0
0.8
0.6
0.4
0.2
0.0
2W
4W
Controls
KASE rats delayed onset
KASE rats regular onset

Figure 8

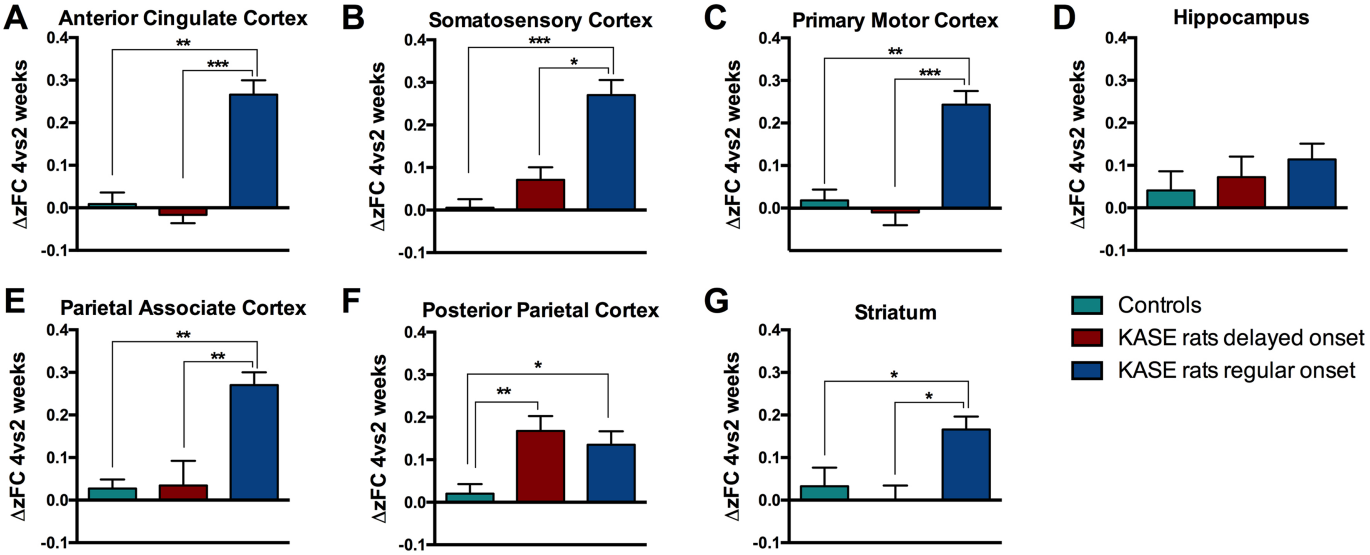
A
Anterior Cingulate Cortex
B
Somatosensory Cortex
C
Primary Motor Cortex
D
Hippocampus
E
Parietal Associate Cortex
F
Posterior Parietal Cortex
G
Striatum
ΔzFC 4vs2 weeks
0.4
0.3
0.2
0.1
0.0
-0.1
**
***
*
Controls
KASE rats delayed onset
KASE rats regular onset

Figure 9